

# PCCP

Accepted Manuscript



This is an *Accepted Manuscript*, which has been through the Royal Society of Chemistry peer review process and has been accepted for publication.

*Accepted Manuscripts* are published online shortly after acceptance, before technical editing, formatting and proof reading. Using this free service, authors can make their results available to the community, in citable form, before we publish the edited article. We will replace this *Accepted Manuscript* with the edited and formatted *Advance Article* as soon as it is available.

You can find more information about *Accepted Manuscripts* in the [Information for Authors](#).

Please note that technical editing may introduce minor changes to the text and/or graphics, which may alter content. The journal's standard [Terms & Conditions](#) and the [Ethical guidelines](#) still apply. In no event shall the Royal Society of Chemistry be held responsible for any errors or omissions in this *Accepted Manuscript* or any consequences arising from the use of any information it contains.

# Revisiting the carbonyl $n \rightarrow \pi^*$ electronic excitation through topological eyes: expanding, enriching and enhancing the chemical language using electron number distribution functions and domain averaged Fermi holes

David Ferro-Costas<sup>\*1</sup>, Evelio Francisco<sup>2</sup>, Ángel Martín Pendás<sup>2</sup>, and Ricardo A. Mosquera<sup>1</sup>

<sup>1</sup>Departamento de Química Física, Universidade de Vigo, Facultade de Química, Lagoas-Marcosende s/n, 36310 Vigo, Spain

<sup>2</sup>Departamento de Química Física y Analítica, Facultad de Química, Universidad de Oviedo, 33006-Oviedo, Spain

## Abstract

The theory of chemical bonding is underdeveloped in electronic excited states, even in small molecules. Fortunately, real space tools may be used to offer rich images of simple excitation processes, as it is shown in this work. The statistics of the electron populations, through a fruitful combination of electron distribution functions (EDFs) and domain averaged Fermi holes (DAFHs), was used to enlighten our chemical knowledge of a paradigmatic process: the  $n \rightarrow \pi^*$  excitation in formaldehyde. Interestingly, our results are perfectly compatible with an alternative perception of the electronic transition: the rotation of one averaged-electron in the oxygen lone pair. This topological model does not require inter-orbital jumps to explain the final electron distribution and, in our humble opinion, this fact makes it, to some extent, more realistic. Finally, other far-reaching conclusions emerge smoothly from our analysis: (i) the  $\sigma$  link may contribute less to the total bond order (as measured by the delocalization index) of a polar double bond than the  $\pi$  one; (ii) populating an antibonding orbital does not necessarily imply decreasing the bond order of its corresponding bond.

**Keywords:** QTAIM, electron distribution function, Fermi hole, excited states, formaldehyde, lone pair rotation, populating antibonding orbitals

---

\*Email: davidferro@uvigo.es; Corresponding author

# 1 Introduction

The power of real space tools to analyze chemical bonding problems is, after several decades of active and intense research, out of question.<sup>[1]</sup> Topological approaches, collectively known as Quantum Chemical Topology (QCT),<sup>[2]</sup> provide orbital invariant indicators that depend neither on the theoretical level, in the case of computational approaches, nor on the experimental techniques used to construct them. It is this property that makes QCT unique among the chemist's interpretative toolbox, on the one hand, but also the root of some of its problems, on the other. Without orbitals, i.e. without effective electrons, the predictive models that lie at the very heart of chemical intuition vanish in thin air, and alternative proposals, we admit, appear at a slow pace. While this gap closes, recourse to QCT compliant methodologies that reintroduce electrons may open new avenues in chemical bonding studies.

Common to many QCT analyses is the exhaustive topological partition of the real space induced by a given invariant field. Well known examples are the atomic partition provided by the electron density ( $\rho$ ), which forms the basis of the Quantum theory of atoms in molecules (QTAIM) developed by R. F. W. Bader and coworkers;<sup>[3,4]</sup> or the partition induced by the electron localization function (ELF) of Becke and Edgecombe<sup>[5]</sup> which was shown to isolate atomic cores, together with bonding and lone pair domains in a landmark study by Savin and Silvi.<sup>[6]</sup> Once a partition of the space is selected, effective electrons may be reintroduced through several procedures.

One possibility is to appeal to the statistical distribution of electrons in the chosen domains. Statistical thinking is at the core of quantum mechanical orthodoxy, but it has been mostly abandoned in chemical reasoning. Chemists are familiar, for instance, with average atomic electron populations, but hardly think in the probability of finding a given partition of the  $N$  electrons of a molecule in those atomic regions. The statistics of that distribution is accessible through the squared modulus of the wave function, and leads to electron distribution functions (EDFs).<sup>[7-11]</sup> If we use QTAIM atomic domains, each partition of the  $N$  electrons leads to a *real space resonance structure* (RSRS), resembling a classical Pauling resonance structure. Through EDFs and RSRS's, integer electrons return to QCT, and new concepts appear that help us to redefine and enhance traditional concepts of chemical bonding theories.

A second possibility is to coarse-grain the exchange-correlation density in a spatial domain. This is the basis of the Domain averaged Fermi hole analysis (DAFH) proposed by R. Ponec.<sup>[12,13]</sup> Diagonalization of the DAFH leads to a set of one-electron functions, or domain natural orbitals (DNOs), that have been shown to provide vivid images of how electrons localize and delocalize in molecules. DNOs are usually close to the standard orbital picture, thus building bridges between the two worlds.

It has also been shown that, at the single-determinant level, DNOs may be understood as statistically independent electrons that reconstruct the full molecular EDF,<sup>[14]</sup> so that a deep link exists between the two techniques. An analysis of the meaning of DAFHs in the case of correlated wave functions has also been reported.<sup>[15]</sup>

The information that can be extracted from these electron recovering techniques is extremely wide and, as previously indicated, it can be used to close (or at least decrease) the predictive gap of many QCT analyses. In this work we will focus on what we can learn from the combined use of EDF and DAFH analyses in formaldehyde. We will scan two- and three-basin distribution functions, paying attention to the decomposition of the former into a direct product of two-center two-electron (2c,2e) links which will be, whenever possible, related to the eigenvectors of the DAFHs. This prototypical system will allow us to strengthen concepts related to the  $\sigma/\pi$  distribution, as well as to refute properties which are standardly, and wrongly, associated to the population of antibonding orbitals. Moreover, we will not limit ourselves to the ground state and, as an example, the first singlet excited state will be also analyzed ( $S_1$ ). It is really noteworthy that, although statistically-based analysis included within QCT have shown to be very valuable to understand key concepts in the Chemistry of ground state molecules, studies analyzing them in electronically excited states (EES's) are actually scarce. Indeed, QTAIM is usually thought of as a theory of ground state molecules and the historical prejudice, based on the appearance of non-nuclear attractors (NNA's) in naïve models of excited states, seemed to preclude the use of QTAIM beyond the electronic ground state.<sup>[16]</sup> However, it is of importance to notice that a large class of chemically important photochemical processes involves excited states which do not show NNA's. As a matter of fact, we have found in a previous work<sup>[17]</sup> that QTAIM is versatile enough to deal with EES's and that its results can expand its simple molecular orbital conception. Thus, the present work is a natural sequel of our previous research.<sup>[17]</sup>

The paper is organized as follows. First we devote a Section to present our basic methods. After considering the computational conditions of our calculations in Section 3 we will discuss our results, first showing the two-basin EDF and DAFH analysis for the ground state, and then generalizing it to the  $S_1$  and  $T_1$  excited states. After a brief consideration of 3-basin EDFs, we close by enumerating the conclusions of our work.

## 2 Methodology

### 2.1 $m$ -basin EDF

Let us consider an exhaustive partition of  $\mathbb{R}^3$  into  $m$  disjoint domains  $\Omega_k$  (i.e.  $\cup_{k=1}^m \Omega_k = \mathbb{R}^3$ ). Given an  $N$ -electron molecular wave function  $\Psi(1, \dots, N)$ , the probability of finding simultaneously  $n_1$  electrons within  $\Omega_1$ ,  $n_2$  within  $\Omega_2$ , ..., and  $n_m$  within  $\Omega_m$  (with  $\sum_{k=1}^m n_k = N$  such that  $n_k \in \mathbb{N}_{\geq 0} \forall k$ ), is given by:<sup>[7]</sup>

$$p_S = \mathcal{N} \int_D |\Psi|^2 d\mathbf{r}_1 d\mathbf{r}_2 \cdots d\mathbf{r}_N \quad (1)$$

where  $S = \{n_1, n_2, \dots, n_m\}$  defines an individual RSRS,  $\mathcal{N}$  accounts for the indistinguishability of electrons ( $\mathcal{N} = N!/\prod_{i=1}^m n_i!$ ), and  $D$  is a multidimensional domain in which the first  $n_1$  electrons are integrated over  $\Omega_1$ , the second  $n_2$  electrons over  $\Omega_2$ , etc. Notice that, for a  $N$ -electron system divided into  $m$  domains, the number of  $p_S$  probabilities (i.e. the number of RSRS's) is given by  $N_S(N, m) = (N + m - 1)!/(N!(m - 1)!)$  and this set of  $N_S$  probabilities defines the EDF of the system. If these  $p_S$  values are ordered in some prescribed way, they can be gathered into an EDF vector  $\mathbf{p}_N$ . Thus, for example, for a A-B 2-center EDF, we could choose a Tartaglia-like order for the  $\mathbf{p}_N$  vector components:  $\mathbf{p}_N = (p_{(n_A=N, n_B=0)}, p_{(n_A=N-1, n_B=1)}, \dots, p_{(n_A=0, n_B=N)})$ .

The importance of analyzing the EDF of a system can be associated, in part, to the definition of diverse important concepts in chemical bonding theory in terms of the  $m$ -basin probabilities. Thus, for instance, the average electron population of a molecular fragment,  $\langle n_A \rangle$ , is given by the integral of the electron density  $\rho(\mathbf{r})$  over the target domain, but it can be also obtained from the EDF terms as the next equation illustrates:

$$\int_{\Omega_A} \rho(\mathbf{r}) d\mathbf{r} = \langle n_A \rangle = \sum_{n_A} n_A p_{n_A} \quad (2)$$

where  $p_{n_A}$  represents the probability of finding  $n_A$  electrons in the domain A whereas the rest of the electrons ( $N - n_A$ ) lie in the complement region. The  $p_{n_A}$  probabilities define a two-basin  $\mathbf{p}_N$  EDF vector, which can be easily obtained from the general  $m$ -basin  $\mathbf{p}_N$  vector according to:

$$p_{n_A} = \sum_{n_B, \dots, n_m} p_{n_A, n_B, \dots, n_m} \quad (3)$$

such that  $\sum_{k=B}^m n_k = N - n_A$ .

In the same vein, the delocalization index (DI) between two fragments A and B ( $\delta_{AB}$ ), which provides us with a measure of the number of electron pairs shared between the two fragments, is defined as:

$$\delta_{AB} = -2 \int_{\Omega_A} \int_{\Omega_B} \rho_2^{xc}(\mathbf{r}_1, \mathbf{r}_2) d\mathbf{r}_1 d\mathbf{r}_2 \quad (4)$$

where  $\rho_2^{xc}$  is the spin-less exchange-correlation pair density. In terms of the EDF, it can be shown that this magnitude can be obtained as:

$$\delta_{AB} = -2 [\langle n_A n_B \rangle - \langle n_A \rangle \langle n_B \rangle] = -2 \left[ \sum_{n_A, n_B} n_A n_B \cdot p_{n_A, n_B} - \sum_{n_A} n_A p_{n_A} \sum_{n_B} n_B p_{n_B} \right] \quad (5)$$

where the probability  $p_{n_A, n_B}$  can be straightforwardly obtained from the general  $m$ -basin  $\mathbf{p}_N$  vector, as it was also previously done for the  $p_{n_A}$  probabilities.

## 2.2 Two-center two-electron links and the two-basin EDF

Often we may be interested only in the bonding between a given domain  $\Omega$ , defined in the molecule, and its complement,  $\Omega' = \mathbb{R}^3 - \Omega$ . Moreover, the definition of as many domains as atoms-in-the-molecule is accompanied by a huge number of RSRS's, whereas the consideration of only two regions decreases this to  $N_S(N, 2) = (N + 2 - 1)! / (N!(2 - 1)!) = N + 1$ . This reduction allows for an easier and interesting analysis of the bonds between regions. Actually, if we demand each bond (for a system of two-centers and multiple two-electron bonds) to be independent of the others, we can decompose any  $\mathbf{p}_{2n}$  EDF vector (with  $2n = N$ ) into the direct product of  $n$   $\mathbf{p}_2$  vectors (i.e. two-electron bonds):<sup>[18]</sup>

$$\mathbf{p}_{2n} = \otimes_{i=1}^n \mathbf{p}_2^i \quad (6)$$

Generally, this decomposition is not unique, *i.e.* eq 6 admits different solutions, and, consequently, various sets of  $\mathbf{p}_2$  vectors can regenerate the original  $\mathbf{p}_{2n}$  EDF vector. Finding the most physically meaningful solution is not always trivial and the chemical knowledge about the system can play a crucial role in such a case.

Each of these individual (2c,2e) links consists of three components:  $p_{2,0}$ ,  $p_{1,1}$ , and  $p_{0,2}$ . As the sum of the three adds to one, we only have two independent variables and, consequently, each  $\mathbf{p}_2$  vector can be characterized through two parameters. A possible choice<sup>[18]</sup> for them is taking as first parameter the probability that one of the bonding electrons lies within domain  $\Omega$ ,  $\pi = p(\Omega) = p_{2,0} + p_{1,1}/2$ . This is equivalent to choosing the electron charge transfer towards basin  $\Omega$  ( $q = 2\pi - 1$ ). The second parameter may now be chosen as the correlation factor  $f$ , that measures the statistical dependence of the electrons in the space and is given by:

$$f = \frac{p_{1,1}}{2\pi(1 - \pi)} - 1 \quad (7)$$

This parameter is the analogue of the standard  $f(\mathbf{r}_1, \mathbf{r}_2)$  used in density matrix theory to express the pair density in terms of the one-body density:  $\rho_2(\mathbf{r}_1, \mathbf{r}_2) = \rho(\mathbf{r}_1)\rho(\mathbf{r}_2)(1 + f(\mathbf{r}_1, \mathbf{r}_2))$ . Interestingly,  $f$

classifies (2c,2e) links into three categories: (i) bonds with statistically independent electrons ( $f = 0$ ), (ii) bonds with electrons negatively correlated in space ( $f > 0$ ), where the location of an electron in the domain  $\Omega$  reduces the probability of finding another electron in the same region, and (iii) bonds with positively correlated electrons ( $f < 0$ ).

With these two parameters, the delocalization index between the two domains associated to the (2c,2e) link takes the form:

$$\delta_{\Omega\Omega'} = (1 - f)(1 - q^2) \quad (8)$$

and, consequently, covalency vanishes at either the  $q = 1$  or  $f = 1$  limits. Moreover, the sum of these individual (2c,2e) delocalization indices reconstructs the total  $\delta_{\Omega\Omega'}$ , associated to the original  $\mathbf{p}_{2n}$ :

$$\delta_{\Omega\Omega'}(\mathbf{p}_{2n}) = \delta_{\Omega\Omega'}(\otimes_{i=1}^n \mathbf{p}_2^i) = \sum_{i=1}^n \delta_{\Omega\Omega'}(\mathbf{p}_2^i) = \sum_{i=1}^n (1 - f_i)(1 - q_i^2) \quad (9)$$

Hence, the contribution of each pair of averaged electrons to the delocalization index can be known as long as we consider that each (2c,2e) link is independent of the others, as it is implicitly assumed by all physical and chemical traditions.

### 2.3 DAFH analysis

The correlation in the position of two electrons can be summarized in the exchange-correlation density hole,  $\rho^{hole}(\mathbf{r}_2|\mathbf{r}_1)$ , which is the difference between the electron density at  $\mathbf{r}_2$  and the conditional density of an electron being at  $\mathbf{r}_2$  when another is known to be at  $\mathbf{r}_1$ :

$$\rho^{hole}(\mathbf{r}_2|\mathbf{r}_1) = \rho(\mathbf{r}_2) - \frac{\rho_2(\mathbf{r}_1, \mathbf{r}_2)}{\rho(\mathbf{r}_1)} \quad (10)$$

where it is of importance to point that we are considering the McWeeny normalization criterion<sup>[19]</sup> for the spinless second order density matrix:

$$\rho_2(\mathbf{r}_1, \mathbf{r}_2) = N(N - 1) \int |\Psi|^2 d\sigma_1 d\sigma_2 dx_3 \dots dx_N \quad (11)$$

where  $x_i$  accounts for both spatial ( $\mathbf{r}_i$ ) and spin ( $\sigma_i$ ) coordinates of the  $i$ -th electron.

Unfortunately, the exchange-correlation hole presents a dependence on the reference electron at  $\mathbf{r}_1$ . Fixing the reference electron at a single point is problematic<sup>[12]</sup> and, in order to deal with such a dependence, Ponec introduced the DAFH, which coarse-grains it by averaging the position of the reference electron over a given spatial domain, generating a more useful and realistic picture. Thus, we have:

$$\rho_{\Omega}^{hole}(\mathbf{r}_2) = \rho(\mathbf{r}_2) - \frac{\int_{\Omega} \rho_2(\mathbf{r}_1, \mathbf{r}_2) d\mathbf{r}_1}{\int_{\Omega} \rho(\mathbf{r}_1) d\mathbf{r}_1} \quad (12)$$

and the charge-weighted DAFH (or just DAFH hereinafter) is defined, then, as  $G^\Omega(\mathbf{r}_2) = N_\Omega \rho_\Omega^{hole}(\mathbf{r}_2)$ , where  $N_\Omega$  is the average electron population associated to the domain  $\Omega$ . Interestingly, the DAFH can be expressed in a simpler form through the exchange-correlation ( $xc$ ) part of the second order density matrix ( $\rho_2^{xc}$ ) as:

$$G^\Omega(\mathbf{r}_2) = \int_\Omega \rho_2^{xc}(\mathbf{r}_1, \mathbf{r}_2) d\mathbf{r}_1 \quad (13)$$

With this, it is useful to decompose this function into one electron contributions. Firstly, we can expand  $\rho_2^{xc}$  in terms of the natural or canonical spin-orbitals ( $\chi_i$ 's) of the molecule as follows:

$$\rho_2^{xc}(\mathbf{r}_1, \mathbf{r}_2) = \sum_{ijkl}^M \eta_{ijkl} \chi_i(\mathbf{r}_1) \chi_j(\mathbf{r}_1) \chi_k(\mathbf{r}_2) \chi_l(\mathbf{r}_2) \quad (14)$$

where the summation limit for the four indices extend to the total number of spin-orbitals ( $M$ ) and the  $\eta_{ijkl}$  terms are expansion coefficients. According to it,  $G^\Omega$  acquires the form:

$$G^\Omega(\mathbf{r}_2) = \sum_{kl}^M \chi_k(\mathbf{r}_2) \cdot \left( \sum_{ij}^M \eta_{ijkl} S_{ij}^\Omega \right) \cdot \chi_l(\mathbf{r}_2) = \sum_{kl}^M \chi_k(\mathbf{r}_2) \cdot G_{kl}^\Omega \cdot \chi_l(\mathbf{r}_2) \quad (15)$$

where the  $S_{ij}^\Omega$  quantities, equal to  $\int_\Omega \chi_i(\mathbf{r}_1) \chi_j(\mathbf{r}_1) d\mathbf{r}_1$ , are the atomic overlap matrix (AOM) elements. The diagonalization of the previous linear form gives rise to:

$$G^\Omega(\mathbf{r}_2) = \sum_k^M n_k^\Omega |\phi_k^\Omega(\mathbf{r}_2)|^2 \quad (16)$$

where  $n_k^\Omega$  is the occupation number of the correlated domain natural orbital (DNO)  $\phi_k^\Omega$  for the domain  $\Omega$ . Due to the fact that the Fermi holes associated with a region are largely localized in the same region, the eigenvectors ( $\phi_k^\Omega$ 's) and eigenvalues ( $n_k^\Omega$ 's) of the  $G^\Omega$  matrix provide a specific and extremely rich source of structural information of the corresponding fragment, such as how electrons are internally distributed within a group, and how they delocalize towards others. Normally, these DAFH eigenvectors are subjected to an isopynic localization,<sup>[20]</sup> but this transformation is not performed here for the sake of convenience, as these orbitals maintain the canonical nature and they can be related to (2c,2e) EDF links.

In terms of the DAFH, the delocalization index between the two domains is given by:

$$\delta_{\Omega\Omega'} = \int_{\Omega'} G^\Omega(\mathbf{r}) d\mathbf{r} + \int_\Omega G^{\Omega'}(\mathbf{r}) d\mathbf{r} \quad (17)$$

and, considering its DNO's, we get:

$$\delta_{\Omega\Omega'} = \sum_k^M n_k^\Omega \int_{\Omega'} |\phi_k^\Omega(\mathbf{r})|^2 d\mathbf{r} + \sum_k^M n_k^{\Omega'} \int_\Omega |\phi_k^{\Omega'}(\mathbf{r})|^2 d\mathbf{r} \quad (18)$$

Taking into account that DNO's are normalized and defining  $s_k^\Omega = \int_\Omega |\phi_k^\Omega(\mathbf{r})|^2 d\mathbf{r}$ , the previous equation can be written as:

$$\delta_{\Omega\Omega'} = \sum_k^M n_k^\Omega (1 - s_k^\Omega) + \sum_k^M n_k^{\Omega'} (1 - s_k^{\Omega'}) \quad (19)$$

Thus, the delocalization index can be expanded in terms of individual contributions, each one associated to a single DNO without crossed-terms between them. In this manner, similarities between DAFH and EDF analysis rise, as both provide us with a chemically-meaningfully decomposition of the delocalization index.

## 2.4 EDF and DAFH relationship

In the absence of electron correlation, it is well-known that the DAFH decomposition can be used to reconstruct the exact EDF.<sup>[14]</sup> Specifically, the occupation number of a given DNO  $n_i^\Omega$  measures the probability, for the effective electron described by this orbital, of being in the region  $\Omega$ . Thus, each  $\phi_i^\Omega$  DNO is endowed with a one-particle EDF vector  $\mathbf{p}_1^i = (n_i^\Omega, 1 - n_i^\Omega)$ . Consequently, the total (2c,2e) EDF can be expressed as:

$$\mathbf{p}_{2n} = \left\{ \otimes_{i=1}^n \mathbf{p}_1^i \right\}_\alpha \otimes \left\{ \otimes_{i=1}^n \mathbf{p}_1^i \right\}_\beta \quad (20)$$

where we clearly separate the set of DNO's associated to  $\alpha$  and to  $\beta$  electrons.\* However, considering the Lewis vision of the electronic structure, it is better to analyze the total EDF in terms of pairs of electrons, in order to understand the bonding structure. For closed-shell systems, it seems chemically intuitive to group the electrons of different spin associated to the same DNO. Doing so, the  $i$ -th DNO can be now related to a  $\mathbf{p}_2^i$  distribution defined by:

$$\mathbf{p}_2^i = \left\{ \mathbf{p}_1^i \right\}_\alpha \otimes \left\{ \mathbf{p}_1^i \right\}_\beta = \left( [n_i^\Omega]^2, 2n_i^\Omega [1 - n_i^\Omega], [1 - n_i^\Omega]^2 \right) \quad (21)$$

Obviously, each of these  $\mathbf{p}_2^i$  distributions is characterized by a null  $f$  parameter, which indicates that the two electrons defining the Lewis pair associated to a given DNO are statistically independent.

As previously indicated, the set of (2c,2e) links used to reconstruct the general  $\mathbf{p}_N$  EDF vector is, in general, not unique (eq 6). Fortunately, the DAFH analysis provides an interesting set of (2c,2e) links, where each element can be endowed with a chemical nature based on orbitals. Unfortunately, this property does not hold for multi-determinant wave functions. In such cases, the  $i$ th eigenvector of the matrix associated to  $G^\Omega$  is not equal, in general, to the corresponding one of its complementary region ( $G^{\Omega'}$ ). Moreover, for multi-determinant wave functions, the set of DNO's consists of more orbitals than electrons, preventing the association of an individual  $\mathbf{p}_1^i$  vector to each DNO in order

\*For the sake of simplicity, we are considering systems with the same number of  $\alpha$  and  $\beta$  electrons

to regenerate the total EDF. As we will demonstrate, the combined use of both EDF and DAFH analyses in multi-determinant cases may be satisfactorily used to enlighten the statistical analysis of the EDF with the widespread chemical terminology.

### 3 Computational details

EDF and DAFH analysis for the ground and first electronically excited states of formaldehyde ( $S_0$ ,  $S_1$ , and also  $T_1$ ) were performed for diverse wave functions computed at the CCSD optimized ground state geometry. The  $S_0$  wave function was obtained using the Hartree-Fock (HF) level and the state-specific (SS) version of the Complete Active Space Self-Consistent Field (CASSCF)<sup>[21]</sup> method. Several active spaces (AS's), enumerated below, were employed:

- AS-I, comprising two electrons and the oxygen lone pair ( $lp$ ) and  $\pi_{CO}^*$  orbitals. This is a (2e,2o) active space.
- AS-II, which is also a (2e,2o) active space, this time including the pair of  $\pi_{CO}$  and  $\pi_{CO}^*$  orbitals.
- Our third choice (AS-III) corresponds to the merge of the previous ones. Namely, a (4e,3o) space involving the pair  $\pi_{CO}/\pi_{CO}^*$  and the oxygen lone pair.
- Finally, AS-IV adds the  $\sigma_{CO}/\sigma_{CO}^*$  duo to the AS-III, giving rise to a (6e,5o) active space.

Since we are interested in the comparison of the  $S_1$  excited and the  $S_0$  ground states, we have decided to analyze both through the state-averaged (SA) version of the CASSCF method. This choice is important in order to obtain a balanced description which does not favor one state over the other. The active spaces employed in this case are the same previously described with the exception of AS-II, for it cannot describe the  $n\pi_{CO}^*$  nature of the  $S_1$  excited state.<sup>†</sup> With regard to the triplet state,  $T_1$ , only the restricted open-shell HartreeFock (ROHF) wave function was obtained.

All the atomic overlap matrices were obtained with PROMOLDEN<sup>[22]</sup> and used as input to the EDF code,<sup>[11]</sup> in order to perform the EDF analysis. A code developed also by the Quantum Chemistry group of Oviedo University was employed for the analysis of the DAFH.

HF, ROHF and CCSD calculations were performed with Gaussian (v09),<sup>[23]</sup> whereas MOLCAS (v7.8) was used for CASSCF ones. The basis set employed in all the calculations is the triple-zeta Dunning basis set cc-pVTZ.<sup>[24]</sup>

<sup>†</sup>We want to notice that the  $n$  in the standard  $n\pi_{CO}^*$  notation accounts for the oxygen lone pair ( $lp$ ).

## 4 Results

### 4.1 Two-basin EDF and DAFH analyses of ground state formaldehyde

In this section we will consider the division of the system into two fragments:  $\Omega$  and its complement  $\Omega'$ . As formaldehyde presents four QTAIM atomic basins, we can define five different partitions in its  $C_{2v}$  optimal arrangement. For the sake of simplicity, we will analyze exclusively one of those, as similar interpretations are obtained from the rest of them (electronic supplementary information). According to traditional knowledge, the fragment involved in more bonds is the C atom and, consequently, we consider that the division defined by the C basin ( $\Omega = \Omega_C$ ) and its complement ( $\Omega' = \Omega_O \cup \Omega_{H1} \cup \Omega_{H2}$ ) is the most attractive.

The eight different DNO's arising from the DAFH decomposition at the HF level are depicted in Figure 1 and each of them is accompanied by three numbers, which describe the associated  $\mathbf{p}_2$  distribution:  $q$ ,  $f$  and the contribution of the orbital to the total  $\delta_{\Omega\Omega'}$  (eq 19). We observe that three of them are extremely localized (as indicated by the absolute value of the  $q$  parameter,  $|q| \sim 1$ ), which clearly resemble the  $1s_O$ ,  $1s_C$  and  $2s_O$  orbitals. Two DNO's account, basically, for the bond between the C basin and the two H basins of the  $\Omega'$  region. Whereas one of these two bonds is polarized toward the C atom ( $a_1$  symmetry), the other ( $b_2$  symmetry) is polarized, almost in the same amount, to the hydrogens. Thus, on average, each individual C-H bond presents a negligible charge transfer (slightly directed towards C), which is in accordance with the hydrogen atomic population (0.991 au). With regard to the CO bond, we observe that both the  $\sigma_{CO}$  and  $\pi_{CO}$  orbitals are strongly polarized towards O (more than half an electron each) and, as a consequence, their contribution to  $\delta_{\Omega\Omega'}$  is smaller than 1.0 au each.

Here we observe that the contribution to the delocalization index is greater for the  $\pi$  orbital (0.6455 au) than for the  $\sigma$  one (0.5263 au). This interesting result can be easily rationalized in terms of electron distributions. As previously indicated, each DNO is characterized by a  $\mathbf{p}_1^i$  vector. This vector is defined by a probability  $n_i^\Omega$  for the electron being in  $\Omega$ . The delocalization index of the corresponding  $\mathbf{p}_2^i$  distribution is given by  $\delta = 4n_i^\Omega(1 - n_i^\Omega)$ , which presents a maximum at  $n_i^\Omega = 1/2$  (Figure 2). Thus, at the HF level, the  $\sigma$  and the  $\pi$  contribution to the delocalization index between identical fragments (for example, in  $H_2CCH_2$ ) are identical and equal to 1.0 au. However, in heteronuclear bonds,  $n_i^\Omega \neq 1/2$  and the more  $n_i^\Omega$  departs from this value, the smaller its contribution to the delocalization index. It seems reasonable to think that orbitals describing the  $\sigma$  bond experience more intensely the effect of the electronegativity difference than  $\pi$  orbitals (as we have observed in a previous work<sup>[25]</sup>). Consequently, for a given AB double bond, the value of  $n_\pi^\Omega$  should be closer to 0.5 than

$n_{\sigma}^{\Omega}$  (for formaldehyde,  $n_{\pi_{CO}}^{\Omega} = 0.202$  whereas  $n_{\sigma_{CO}}^{\Omega} = 0.156$ ) and, consequently, in heteronuclear double bonds the  $\pi$  orbital contributes more to the delocalization between the bounded fragments. Finally, we also observe that the oxygen lone pair, although greatly localized in the oxygen basin, also contributes significantly (0.053 au) to the delocalization index.

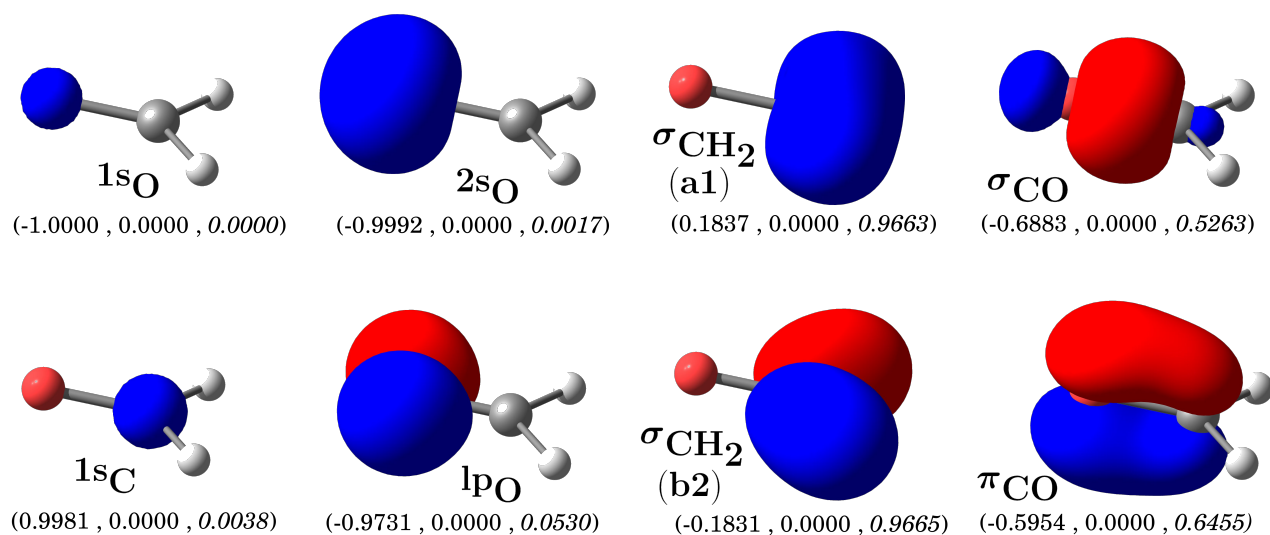


Figure 1: DNOs for formaldehyde at the HF/cc-pVTZ level of calculation. The triad of numbers in each orbital corresponds, in order, to the  $q$  and  $f$  parameters associated to the corresponding  $\mathbf{p}_2$  distribution, and to the contribution to the delocalization index (in *italic*) between the C basin and its complement.

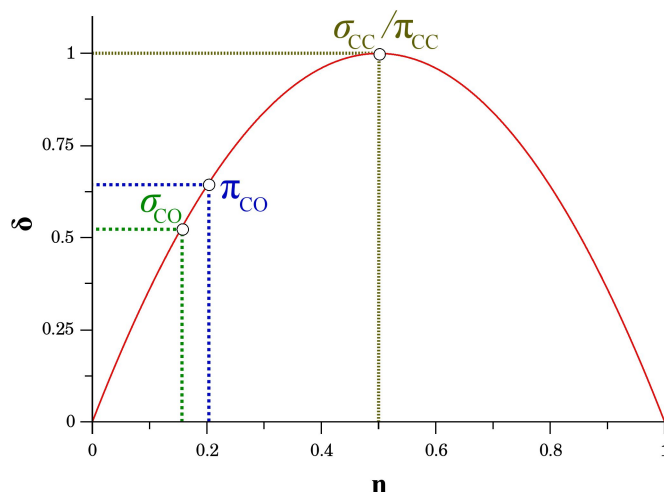


Figure 2: Variation of the DNO contribution to the delocalization index ( $\delta$ ) between the domain  $\Omega$  and its complement ( $\Omega'$ ) with regard to its occupation number ( $\mathbf{n}$ ). The parabolic behavior results from the association of a  $\mathbf{p}_2$  vector to the DNO in closed-shell HF calculations.

At this point, we want to highlight two points. Firstly, the decomposition of the delocalization index between  $\Omega$  and  $\Omega'$  does not present crossed terms when DNO's are employed (i.e.,  $s_{ij}^{\Omega} = s_{ij}^{\Omega'} = 0$  for  $i \neq j$ , where  $s_{ij}^{\Omega} = \langle \phi_i | \phi_j \rangle_{\Omega}$ ). In general, canonical orbitals arising from standard HF calculations present nonzero values for  $s_{ij}^{\Omega}$  and, consequently, the delocalization index does not depend, exclusively, on  $s_{ii}^{\Omega}$  terms. Thus, pure  $\sigma_{CO}$  and  $\pi_{CO}$  contributions to the delocalization index can be invoked when working with DNO's. Secondly, these DNO's are not as extremely localized, in a QTAIM basin or between a pair of QTAIM basins, as they look like in the Figure. Thus, for example, the two DNO's associated to the C-H bonds are not only defined in the  $\Omega_C \cup \Omega_{H1} \cup \Omega_{H2}$  region, but also in  $\Omega_O$ . Consequently, the estimation of  $\delta_{CH}$  using these orbitals would generate a value of 0.9664 au, whereas the actual value is smaller (0.8981 au). This limitation is a consequence of the 2-basin character of the DAFH analysis, which decomposes the electron density lying in a real region  $\Omega$  and in its complementary fragment, and clearly indicates a non-negligible three-center contribution.

As pointed out in the Methodology section, the DAFH analysis is equivalent, at the HF level, to the decomposition of the total EDF distribution (in this case, the  $\mathbf{p}_{16}$  vector) into a direct product of  $\mathbf{p}_2$  distributions. However, we show here that it is normally common and sufficient to deal with a lower-order distribution vector in order to account for the bonding links between the  $\Omega$  and  $\Omega'$  real space fragments. Thus, for example, more than 99.99% of the probability is collected in a  $\mathbf{p}_8$  vector. The decomposition of this vector provides us with a similar picture of the bonding between the fragments. However, the four (2c,2e) links obtained in this manner present negative values for the

$f$  parameter (Table 1). This fact should be taken into account if partial EDFs are considered: their analysis can generate bonds with negatively ( $f > 0$ ) or positively ( $f < 0$ ) correlated electrons even for closed-shell systems described at a HF level, where the full picture would generate bonds with statistically independent electrons ( $f = 0$  for each link). However, when the omitted  $\mathbf{p}_2$  distributions are characterized by zero  $\delta$  values, the spurious values for the  $f$  parameter disappear, as it can be seen from the  $\mathbf{p}_{14}$  case in Table 1, where the same picture (as with  $\mathbf{p}_{16}$ ) of statistically independent (2c,2e) links is regenerated.

Table 1: Set of  $q$  and  $f$  values associated to the  $\mathbf{p}_2$  distributions arising from the decomposition of  $\mathbf{p}_8$  to  $\mathbf{p}_{14}$  EDF vectors. The decomposition of the  $\mathbf{p}_{16}$  vector is shown in Figure 1.

	$p_8$		$p_{10}$		$p_{12}$		$p_{14}$	
	q	f	q	f	q	f	q	f
$p_2^1$	-0.179	-0.003	-0.183	0.000	-0.183	0.000	-0.183	0.000
$p_2^2$	0.187	-0.005	0.184	0.000	0.184	0.000	0.184	0.000
$p_2^3$	-0.486	-0.034	-0.630	-0.012	-0.595	0.000	-0.595	0.000
$p_2^4$	-0.779	-0.100	-0.661	0.027	-0.689	0.000	-0.688	0.000
$p_2^5$			0.033	0.928	-0.972	0.001	-0.973	0.000
$p_2^6$					0.998	0.000	0.998	0.000
$p_2^7$							-0.999	0.000

Now that the 2-basins analysis is clear at the HF level, we can analyze the effect of electron correlation in both the DAFH and EDF analyses. It is important to realize that, for multiconfigurational wave functions, the total EDF cannot be restored from the DAFH analysis of the system. Consequently, attributing an orbital nature (in terms of the DAFH decomposition) to each  $\mathbf{p}_2$  arising from the EDF distribution is, hence, not longer strict. Nonetheless, as we will see, the values of the delocalization index contribution of each DNO and the delocalization index associated to each  $\mathbf{p}_2$  can be clearly related for AS-I to AS-IV and, therefore, we will preserve the orbital nature to endow the  $\mathbf{p}_2$  vectors with chemical significance.

The contribution of each DNO to the delocalization index is shown in Table 2. We observe that, for a SS-CASSCF(2,2) calculation including the oxygen lone pair and the  $\pi^*$  orbital in the active space (AS-I), the contribution associated to the  $\pi_{CO}^*$  is really small and that the differences with regard to the HF calculation (Figure 1) are basically negligible, except for that of  $\pi_{CO}$ , which increases 0.0024 au. Interestingly, despite the fact that an antibonding orbital has been introduced in the active space, the delocalization index between  $\Omega$  and  $\Omega'$  slightly increases from 3.1630 au (at HF level)

to 3.1658 au. This result is conceptually important and one of the messages of this contribution: populating an antibonding orbital does not necessarily decrease the delocalization index between the corresponding bonded atoms. The decrease appears when the population is removed from orbitals which contribute more to the bond. In this case, the oxygen lone pair decreases its population in order to introduce the  $\pi_{CO}^*$  orbital and it is perfectly feasible that the antibonding orbital contributes more than the lone pair to the electron delocalization. The opposite result can be obtained through a SS-CASSCF(2,2) calculation including the  $\pi_{CO}$  orbital instead of the oxygen lone pair (AS-II), in which case the delocalization index between the two regions decreases, indeed, to 3.0945 au. As it can be foreseen from the previous results, the consideration of the three orbitals (AS-III:  $lp_O$ ,  $\pi_{CO}$  and  $\pi_{CO}^*$ ) barely modifies the AS-II results. When we move to more elaborated active spaces (such as AS-IV), we clearly observe how electron correlation affects more (2c,2e) links. Specifically, both the  $\sigma_{CO}$  and  $\pi_{CO}$   $\mathbf{p}_2$  links describe now two negatively correlated electrons. Interestingly, we observe how the electron correlation is still well localized, as it does not spread its influence to (2c,2e) links which are not included in the active space. And what we feel even more important, the correlation factor associated to the oxygen lone pair orbital is basically zero. This is a topological indication that the inclusion of the corresponding orbital in the active space is, certainly, not worthy. In the same manner, the correlation factor is more relevant for the  $\pi_{CO}$   $\mathbf{p}_2$  vector than for the  $\sigma_{CO}$  one, which indicates that, in this system, electronic correlation plays a more significant role in the  $\pi$  electronic skeleton.

## 4.2 An statistically idyllic picture of the transition to the $(n\pi^*)^1$ state

After understanding the EDF distribution in the ground state of formaldehyde, we are prepared to go a step further: the analysis of electronically excited states. Concretely, our target is the first singlet excited state ( $S_1$ ) of formaldehyde, normally denoted by  $(n\pi^*)^1$ . However, before analyzing any actual result, it is of interest to consider an idyllic picture of the electronic transition to  $(n\pi^*)^1$  and to discuss its properties.

As pointed out before, the  $S_1$  state of formaldehyde is normally invoked as  $(n\pi^*)^1$ . This notation, based on a molecular orbital language, implies the next approximations: (i) the electronic excitation  $S_0 \rightarrow S_1$  brings into play just a single electron (on average) without influencing the rest of them to a large extent, (ii) after the transition, the electron which was described by the oxygen lone pair orbital is now described by the  $\pi$  antibonding molecular orbital associated to the carbonyl bond. From a statistical point of view, both approximations would imply the modification of a single  $\mathbf{p}_1$  vector of those conforming the  $\mathbf{p}_{16}$  EDF vector. From a simple chemical perspective, each electron defining

Table 2: Contribution of each DNO to the delocalization index between  $\Omega$  and its complementary region for SS-CASSCF wave functions (the nature of the active orbitals is indicated between square brackets). The set of  $\mathbf{p}_2$  distributions which corresponding  $\delta$  values resemble most the DAFH decomposition are also shown. For each of them, the  $\delta$  value and the  $q$  and  $f$  parameters are also indicated.

$i$	$\phi_i$ nature	CASSCF(2,2) [lp, $\pi^*$ ]				CASSCF(2,2) [ $\pi,\pi^*$ ]			
		$\delta_{\Omega\Omega'}^i$	$\delta(\mathbf{p}_2^i)$	$q^i$	$f^i$	$\delta_{\Omega\Omega'}^i$	$\delta(\mathbf{p}_2^i)$	$q^i$	$f^i$
1	$1s_O$	0.0000	0.0000	-1.0000	0.0000	0.0000	0.0000	-1.0000	0.0000
2	$2s_O$	0.0017	0.0017	-0.9992	0.0000	0.0017	0.0017	-0.9992	0.0000
3	$1s_C$	0.0038	0.0038	0.9981	0.0000	0.0038	0.0038	0.9981	0.0000
4	$lp_O$	0.0534	0.0527	-0.9733	0.0000	0.0519	0.0519	-0.9737	0.0000
5	$\sigma_{CO}$	0.5260	0.5260	-0.6885	0.0000	0.5233	0.5233	-0.6904	0.0000
6	$\pi_{CO}$	0.6479	0.6489	-0.5928	-0.0003	0.5678	0.5817	-0.5027	0.2216
7	$\sigma_{CH_2}$ (a1)	0.9663	0.9663	0.1835	0.0000	0.9689	0.9689	0.1765	0.0000
8	$\sigma_{CH_2}$ (b2)	0.9664	0.9664	-0.1832	0.0000	0.9633	0.9633	-0.1916	0.0000
9	$\pi_{CO}^*$	0.0002	-	-	-	0.0139	-	-	-
10	$\sigma_{CO}^*$	-	-	-	-	-	-	-	-

$i$	$\phi_i$ nature	CASSCF(4,3) [lp, $\pi,\pi^*$ ]				CASSCF(6,5) [lp, $\sigma,\sigma^*,\pi,\pi^*$ ]			
		$\delta_{\Omega\Omega'}^i$	$\delta(\mathbf{p}_2^i)$	$q^i$	$f^i$	$\delta_{\Omega\Omega'}^i$	$\delta(\mathbf{p}_2^i)$	$q^i$	$f^i$
1	$1s_O$	0.0000	0.0000	-1.0000	0.0000	0.0000	0.0000	-1.0000	0.0000
2	$2s_O$	0.0017	0.0017	-0.9991	0.0000	0.0044	0.0013	-0.9993	-0.0002
3	$1s_C$	0.0038	0.0038	0.9981	0.0000	0.0030	0.0031	0.9984	0.0000
4	$lp_O$	0.0524	0.0514	-0.9740	-0.0001	0.0548	0.0464	-0.9765	-0.0002
5	$\sigma_{CO}$	0.5231	0.5231	-0.6906	0.0000	0.4915	0.5275	-0.6657	0.0526
6	$\pi_{CO}$	0.5685	0.5835	-0.5015	0.2205	0.5628	0.5307	-0.4947	0.2973
7	$\sigma_{CH_2}$ (a1)	0.9688	0.9688	0.1766	0.0000	0.9696	0.9697	0.1741	0.0000
8	$\sigma_{CH_2}$ (b2)	0.9634	0.9635	-0.1910	0.0000	0.9631	0.9631	-0.1922	0.0000
9	$\pi_{CO}^*$	0.0141	-	-	-	0.0001	-	-	-
10	$\sigma_{CO}^*$	-	-	-	-	-0.0096	-	-	-

the oxygen lone pair should be, basically, localized in the oxygen atom, which allows us to write (within this model picture)  $\mathbf{p}_1^{lp} = (0, 1)$ . In this manner, the actual lone pair would be given by  $\mathbf{p}_2^{lp} = (0, 1) \otimes (0, 1) = (0, 0, 1)$ . After the electronic excitation, one of these  $\mathbf{p}_1$  distributions changes. For the statistical description of the  $\pi_{CO}^*$  electron, we can consider a general vector  $\mathbf{p}_1 = (a, 1 - a)$ , where  $a$  accounts for the amount of the electron which is transferred to the C basin. In accordance, we can consider two limiting cases here: one where the electron is essentially located in the C basin ( $a \rightarrow 1$ ), and other where the electron can be found equally within both atoms ( $a \rightarrow 1/2$ ). A third possibility, where we would locate the electron within the oxygen basin ( $a \rightarrow 0$ ), lacks chemical meaning.

With the previous model distributions, we are in a position to analyze the effect of the electronic transition. Before it occurring, the (2c,2e) distribution described by the lone pair is characterized by the parameters  $q_{GS} = -1$  and  $f_{GS} = 0$ , where the subscript *GS* makes reference to the ground state. Once the electronic transition takes place, the (2c,2e) links changes to  $\mathbf{p}_2^{n\pi^*} = (0, 1) \otimes (a, 1 - a) = (0, a, 1 - a)$ , which corresponds to  $q_{ES} = a/2$  and  $f_{ES} = a/(2 - 1)$  (*ES* accounting for the target excited state). The variation in the delocalization index between the C basin and its complement is, then, given by  $\Delta\delta = \delta_{ES} - \delta_{GS} = 2a(1 - a)$  (see eq 8). In this manner, we have arrived to another interesting and unexpected result: the electronic excitation, according to the idyllic ( $n\pi^*$ )<sup>1</sup> notation, should be accompanied by an increase (for  $0 \leq a \leq 1$ ) of the delocalization index between the carbon atom and its complementary domain ( $\Delta\delta_{\Omega\Omega'} > 0$ ). Nevertheless, it is perfectly known<sup>[17]</sup> that the delocalization index decreases upon electronic excitation, a fact that lies also in line with the CO distance increase observed when going to the  $S_1$  excited state. This is why our result is unexpected, but... why is it interesting? Firstly, we have considered an statistically vision of the electronic transition in terms of its commonly used basic molecular orbital description. In terms of it, it is chemically appealing to state that the delocalization index should decrease, as an antibonding orbital is being populated. But... should the delocalization index really decrease as a consequence of such an event? Is then our statistical reasoning wrong? The answer to both questions is actually “No” and the proof is quite straightforward: the delocalization index increases at the SA-CASSCF(AS-I) level (see next subsection). In this calculation only both the lone pair and the  $\pi_{CO}^*$  orbitals define the active space and the output wave function is basically described by one configuration which resembles (we could almost say that corresponds to) our model picture. Only when the active space comprises more orbitals (see next subsection) does the delocalization index decrease. Therefore, the textbook reasoning normally invoked to understand this electronic transition is incorrect, but leads to the correct answer (a decrease of  $\delta_{CO}$ ). This substantiates our claim that our result is interesting: it exemplifies how sometimes we (the chemistry community) tend to endow some chemical entities with a wrong

meaning but, due to the (fortuitous) fact that the final result corresponds to the observed behavior, the concept is not revised/redefined or questioned.

The final idea of this subsection, supplements our previous simple result: the population of an AB antibonding orbital does not imply a decrease in the delocalization index between the A and B domains. Thus, in the simple case of the SA-CASSCF(AS-I) calculation, the antibonding orbital contributes more to  $\delta_{\Omega\Omega'}$  than an electron described by an oxygen lone pair orbital and, consequently,  $\delta_{\Omega\Omega'}$  increases at this level of theory.

### 4.3 Two-basin EDF and DAFH analysis of $S_1$ and $T_1$ states of formaldehyde

Although the effect of the electronic excitation to  $S_1$  on the two-basin EDF looks similar regardless the chosen active space (Figure 3), actually the model picture is only approximately recovered with AS-I, as previously indicated. Roughly, its corresponding EDF distribution is displaced, upon excitation, one electron to increasing values of  $n_C$ , leading to an increase of one electron in the C electron population expected value (concretely, 0.906 au). Taking the  $a$  parameter of the previous section as the increase of  $N_\Omega$ , we obtain an idyllic  $\Delta\delta = 0.170$  au, which is close to the actual computed value, 0.142 au. Nevertheless, this model does not hold for more elaborated active spaces (as AS-III and AS-IV), where the transfer of electron density to the C basin does not increase the delocalization index (Table 4).<sup>[17]</sup>

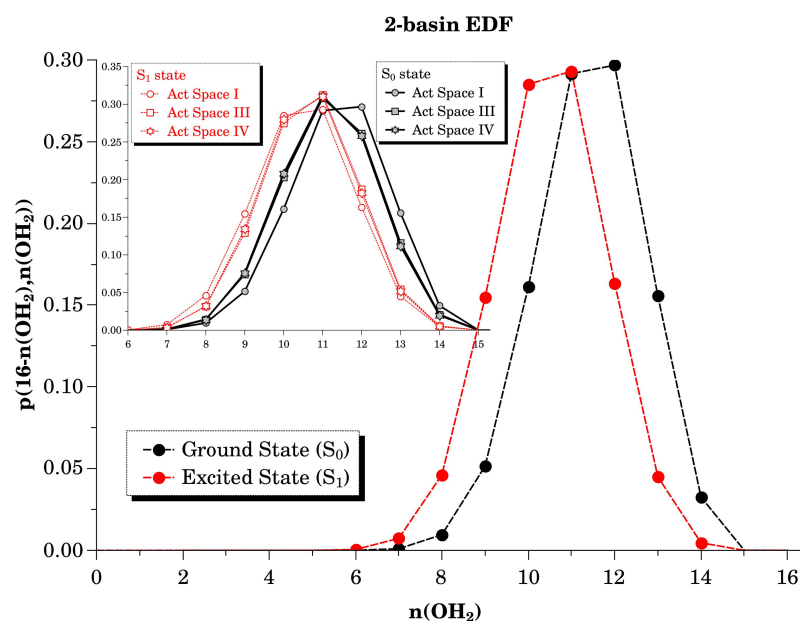


Figure 3: Two-basin EDF distributions for the ground and the first singlet excited states of formaldehyde at the SA-CASSCF(AS-I)/cc-pVTZ level of calculation. In general terms, the distribution for the excited state seems to be displaced one electron to the left. A plot including the three active spaces (AS-I, AS-III and AS-IV) is included in the upper-left corner.

The next logical step in this section would be the analysis of the (2c,2e) link decomposition of the EDF, associating each of these links to an orbital entity: the DAFH eigenvectors. However, due to the multideterminant description of the  $S_1$  state through CASSCF calculations, its EDF cannot be reconstructed exactly from the DAFH eigenvalues, not even using the modest AS-I. Interestingly, both  $S_1$  and the first triplet state,  $T_1$ , are characterized by the same basic orbital nature: a  $n \rightarrow \pi_{CO}^*$  transition.<sup>[17]</sup> Furthermore, a sufficiently good one-determinant approximation to the wave function of the  $T_1$  state of two- $\alpha$  unpaired electrons can be obtained through the ROHF method. Hence, the EDF of  $T_1$  can be decomposed into (2c,2e) links with DAFH significance and this identification can be extrapolated to the  $S_1$  case, in order to better understand its EDF.

The diagonalization of the DAFH for  $\alpha\alpha$ - $T_1$  gives rise to nine  $\alpha$ -DNO's and seven  $\beta$ -DNO's (Figure 4). Comparing them with those for the ground state (Figure 1), we may understand the electronic transition according to two alternative models:

- **Inter-Orbital Jumping (IOJ)** model (Figure 5a). This corresponds to the well established interpretation of the transition. The  $\beta$  electron in the oxygen lone pair jumps to the  $\alpha$   $\pi^*$  spin-orbital. After the transition, the set of  $\alpha$ -spinorbitals contains one electron in a  $\pi$  orbital and another in the  $\pi^*$ . The DAFH machinery is known to provide valence states of the atoms<sup>[12]</sup> and this is a clear example: when both orbitals are populated, Pauli's principle forces a combination

of both the  $\pi$  and  $\pi^*$  orbitals and localizes the electrons, one within each basin, giving rise to electron topological distributions reminding the  $p_z$  atomic orbitals (denoted as  $lp_C^\pi$  and  $lp_O^\pi$  in Figure 4). On the other side, no antibonding orbital is included in the  $\beta$ -spinorbital set, and the  $\beta$ -contribution to the  $\pi$  bond remains almost invariant.

- **Electron Density Rotation (EDR) model** (Figure 5b). The distribution of one electron described by a  $lp_O$  orbital can be considered to rotate 90 degrees (giving rise to the  $lp_C^\pi$ ). Concomitantly, the electron density of the  $\pi_{CO}$  is transferred towards the carbon basin, as a consequence of the new repulsion in the “ $\pi$  cloud”. This transference gives rise to an electron in a C lone pair orbital ( $lp_C^\pi$ ).

We want to highlight that both models are plausible interpretations to understand the electronic transition and they are perfectly compatible. Whereas IOJ can be considered as the “classical” model based on the standard interpretation, the EDR model presents a more attractive image from the topological point of view (see below).

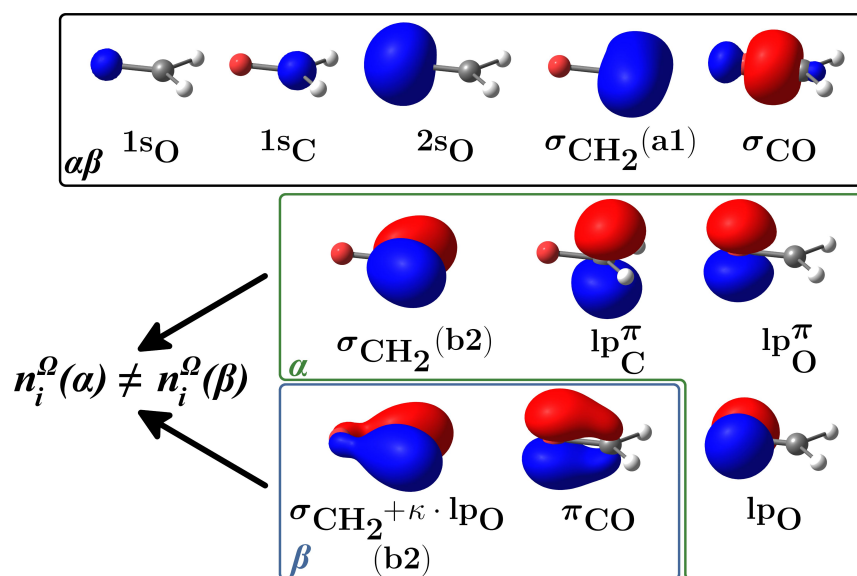


Figure 4: DNOs for the  $\alpha\alpha T_1$  state of formaldehyde at the ROHF/cc-pVTZ level of calculation. Each orbital inside the  $\alpha\beta$  box is related to a  $\mathbf{p}_2^i$  distribution (these  $\alpha$  and  $\beta$  spin-DNO's are equivalent and present the same DAFH eigenvalue), whereas those in boxes  $\alpha$  and  $\beta$  only correspond to one average electron each (i.e., a  $\mathbf{p}_1^i = (n_i^\Omega, 1 - n_i^\Omega)$  distribution).

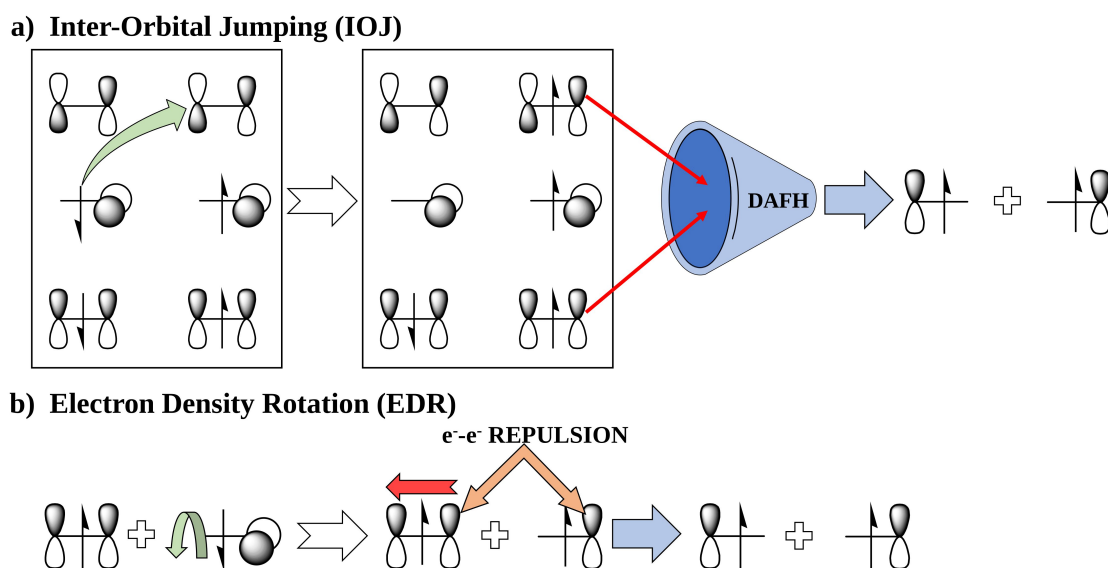


Figure 5: Inter-Orbital Jumping and Electron Density Rotation models for understanding the  $S_0 \rightarrow S_1$  transition in formaldehyde.

Finally, we notice that one electron of the  $\sigma_{CH_2}$  (a1) is slightly polarized towards oxygen, as a consequence of the electron density deficiency caused by the rotation/jumping of one lone pair electron. Its description can be written as  $\sigma_{CH_2} + \kappa \cdot lp_O$ , where  $|\kappa| \ll 1$ .

As chemically expected, those orbitals not involved in the previous process can be matched up in five pairs, each one sharing the same DAFH eigenvalue (those in the  $\alpha\beta$  box of Figure 4). The rest of them can be paired according the previous steps:  $(lp_O, lp_O^\pi)$ ,  $(\pi_{CO}, lp_C^\pi)$  and  $(\sigma_{CH_2}, \sigma_{CH_2} + \kappa \cdot lp_O)_{b2}$ . In this manner, we can observe the effect of the electronic excitation in each original (2c,2e) link (Table 3), quantifying the effect of each of the above steps on chemical bonding.

Upon excitation, the  $q$  and  $\delta$  parameters for the links with  $f = 0$  (associated to those DNO's with the same DAFH eigenvalue) are almost identical and differences do not exceed 0.04 in  $q$  and 0.02 in  $\delta$ . Interestingly, although the DNO topology of one averaged electron corresponding to the oxygen lone pair rotates 90 degrees, its effect on the charge and on the correlation factor is negligible (Figure 1 and Table 3). In our opinion, the fact that no correlation is introduced in the oxygen lone pair chemically supports the fact that the excitation can be better interpreted as a rotation instead of as a  $n \rightarrow \pi_{CO}^*$  transition, as we observed in a previous work.<sup>[17]</sup> However, whereas the rotation observed in this previous work (with the ELF analysis) seems to be associated to the two electrons of the oxygen lone pair, the DAFH analysis throws light on this process, indicating that only one of the two averaged electrons actually rotates. The biggest effect of the excitation corresponds to the

$\pi_{CO}$  link. This link is the only one characterized with a significant (and large) correlation factor. Therefore, the correlation effects associated to the electronic transition concentrate in a single (2c,2e) link. Its delocalization index decrease notoriously (-0.1348 au) and accounts for 92% of the total  $\Delta\delta_{\Omega\Omega'}$  (-0.1464 au). Finally, the polarization of one of the electrons of the  $\sigma_{CH_2}$  (b2) link produces a small effect in its  $\mathbf{p}_2$  distribution parameters, even in the correlation factor, which remains close to zero ( $f = 0.0003$ ).

Table 3: Orbital nature of the (2c,2e) links (EDF decomposition) according to the DAFH analysis (see Figure 4 for DNO nomenclature) of the  $T_1$  state described at ROHF level. The  $(q, f, \delta)$  triad associated to each  $\mathbf{p}_2$  distribution is also shown, as well as the  $q$  parameter variations with regard to those of  $S_0$  described at HF level (Figure 1).

$\mathbf{p}_2^{ij} = \mathbf{p}_1(\phi_i) \otimes \mathbf{p}_1(\phi_j)$	$(n_i^\Omega, n_j^\Omega)$	$q_{ij}$	$f_{ij}$	$\delta_{ij}$	$q(T_1) - q(S_0)$
$[1s_O]^\alpha \otimes [1s_O]^\beta$	(0.0000, 0.0000)	-1.0000	0.0000	0.0000	0.0000
$[2s_O]^\alpha \otimes [2s_O]^\beta$	(0.0006, 0.0006)	-0.9988	0.0000	0.0024	0.0004
$[1s_C]^\alpha \otimes [1s_C]^\beta$	(0.9990, 0.9990)	0.9980	0.0000	0.0040	-0.0001
$[lp_O]^\alpha \otimes [lp_O^\pi]^\alpha$	(0.0132, 0.0136)	-0.9732	0.0000	0.0529	-0.0001
$[\sigma_{CO}]^\alpha \otimes [\sigma_{CO}]^\beta$	(0.1513, 0.1513)	-0.6973	0.0000	0.5137	-0.0090
$[lp_C^\pi]^\alpha \otimes [\pi_{CO}]^\beta$	(0.8167, 0.1201)	-0.0633	0.4872	0.5107	0.5321
$[\sigma_{CH_2}]^\alpha \otimes [\sigma_{CH_2}]^\beta(a_1)$	(0.6111, 0.6111)	0.2223	0.0000	0.9506	0.0386
$[\sigma_{CH_2}]^\alpha \otimes [\sigma_{CH_2} + \kappa \cdot lp_O]^\beta(b_2)$	(0.4425, 0.4254)	-0.1321	0.0003	0.9823	0.0510

With the orbital character associated to each (2c,2e) link in the  $T_1$  state, we are in disposition to understand the  $S_1$  EDF decomposition. As we can see in Table 4, we can find a decomposition of the  $\mathbf{p}_{16}$  distribution which reminds the DAFH one associated to  $T_1$  for each active space. The similarity of values between them indicates that the electronic nature of both  $S_1$  and  $T_1$  is actually similar. Moreover, in both  $S_0$  and  $S_1$ , correlation effects are basically concentrated on the  $\pi$  link, except in the AS-IV, where the  $\sigma_{CO}$  link is also characterized by a significant correlation factor. We consider that there is no need of presenting more exhaustive analyses here, as the data show the same trends found for the excitation to the triplet state, with the exception of the previously indicated increase of the  $\delta_{\Omega\Omega'}$  found for the modest AS-I space.

Table 4: Two-center two-electron distributions, described by the  $(q, f, \delta)$  triad, generated in the decomposition of the  $\mathbf{p}_{16}$  distribution for  $S_0$  and  $S_1$ , both described with the state averaged version of the CASSCF methodology at different active spaces. Their orbital correspondence is based on the similarities with the DAFH analysis of the HF and ROHF wave functions of  $S_0$  and  $T_1$ .

	AS-I			AS-III			AS-IV		
Ground State ( $S_0$ )									
	$q$	$f$	$\delta$	$q$	$f$	$\delta$	$q$	$f$	$\delta$
$1s_O$	-1.0000	0.0000	0.0000	-1.0000	0.0000	0.0000	-1.0000	0.0000	0.0000
$2s_O$	-0.9993	0.0000	0.0015	-0.9992	-0.0001	0.0016	-0.9993	0.0002	0.0015
$1s_C$	0.9978	0.0000	0.0043	0.9979	0.0000	0.0042	0.9984	0.0000	0.0033
$lp_O$	-0.9745	0.0000	0.0503	-0.9757	0.0000	0.0479	-0.9754	-0.0001	0.0487
$\sigma_{CO}$	-0.7174	0.0000	0.4853	-0.7085	0.0000	0.4980	-0.6731	0.0503	0.5195
$\pi_{CO}$	-0.6639	-0.0009	0.5597	-0.4412	0.2513	0.6029	-0.4491	0.3331	0.5324
$\sigma_{CH_2}(b_2)$	-0.2051	0.0000	0.9579	-0.1927	0.0000	0.9628	-0.1954	0.0000	0.9618
$\sigma_{CH_2}(a_1)$	0.1535	0.0000	0.9764	0.1642	0.0000	0.9730	0.1595	0.0000	0.9746
$\sum_i \delta_{\Omega\Omega'}(\mathbf{p}_2^i)$ :			3.0354			3.0906			3.0417
Excited State ( $T_1$ )									
	$q$	$f$	$\delta$	$q$	$f$	$\delta$	$q$	$f$	$\delta$
$1s_O$	-1.0000	0.0000	0.0000	-1.0000	0.0000	0.0000	-1.0000	0.0000	0.0000
$2s_O$	-0.9987	0.0000	0.0025	-0.9987	0.0000	0.0025	-0.9988	0.0000	0.0023
$1s_C$	0.9982	0.0000	0.0036	0.9981	0.0000	0.0038	0.9983	0.0000	0.0034
$lp_O \otimes lp_O^\pi$	-0.9660	0.0001	0.0668	-0.9714	0.0002	0.0563	-0.9711	0.0003	0.0570
$\sigma_{CO}$	-0.6699	0.0000	0.5512	-0.6794	0.0000	0.5385	-0.6796	0.1338	0.4662
$lp_C^\pi \otimes \pi_{CO}$	0.0195	0.3627	0.6370	-0.1039	0.5454	0.4497	-0.0734	0.5097	0.4876
$\sigma_{CH_2}(b_2)$	-0.1383	0.0010	0.9799	-0.1408	0.0002	0.9800	-0.1426	0.0001	0.9795
$\sigma_{CH_2}(a_1)$	0.2529	0.0000	0.9361	0.2268	0.0000	0.9485	0.2233	0.0000	0.9501
$\sum_i \delta_{\Omega\Omega'}(\mathbf{p}_2^i)$ :			3.1770			2.9793			2.9463

Finally, to close this subsection, we have a few words related to the electronegativity variation upon excitation. The  $g_{\Omega\Omega'}$  electronegativity index,<sup>[26,27]</sup> which is a measure of the effective electronegativity difference between  $\Omega$  and  $\Omega'$  for a given bond, is defined as:

$$g_{\Omega\Omega'} = \frac{N_{\Omega\Omega'}^{\Omega} - N_{\Omega\Omega'}^{\Omega'}}{N_{\Omega\Omega'}^{\Omega} + N_{\Omega\Omega'}^{\Omega'}} \quad (22)$$

where  $N_{\Omega\Omega'}^{\Omega}$  and  $N_{\Omega\Omega'}^{\Omega'}$  account for the  $\Omega$  and  $\Omega'$  contributions, respectively, of electron population associated to the target bond between both domains. EDF analyses allow for an immediate decomposition of this index. Thus, the distribution of the two electrons associated to the  $i$ -th (2c,2e) bond

defines a  $g_{\Omega\Omega'}^i$  according to:

$$g_{\Omega\Omega'}^i = \frac{2\pi_i - (2 - 2\pi_i)}{2\pi_i + (2 - 2\pi_i)} = 2\pi_i - 1 = q_i \quad (23)$$

and we notice that, interestingly, the  $q_i$  value associated to the  $\mathbf{p}_2^i$  distribution actually corresponds to the  $g_{\Omega\Omega'}$  electronegativity index. Moreover, as these (2c,2e) links are quite localized between two atomic basins (according to the shape of the corresponding DNO), we can approximate the value of  $q_i$  to the index describing the electronegativity difference between the atoms involved in the described bond. Thus, we observe that the  $q_i$  values associated to the  $a_1$  and  $b_2$  C-H bonds in  $S_1$  (or in  $T_1$ ) increase with regard to  $S_0$ , as well as the associated to the  $\pi$  CO bond (Tables 3 and 4). Consequently, we can state that the relative electronegativity of C has increased upon excitation.

#### 4.4 3-basin EDF and DAFH analysis of formaldehyde

In previous sections we have seen that the distribution of electrons between different domains can be understood in terms of orbitalic entities. This achievement was possible thanks to the relationship between the two-basin EDF and the DAFH eigenvalues and eigenvectors for monodeterminantal systems. However, an EDF analysis is not only useful when the orbital language is present. Not all the information in the realm of Chemistry is endowed with an orbital significance and, concretely, the efforts made so far in the field of the topological approaches have shown that many chemical properties can be understood without invoking orbitals. As an example, this final discussion section concerns the analysis of a three-basin EDF, where an interesting theoretical processes will be analyzed and where EDF results will not be related to any orbital entity.

Considering the  $\Omega_C$ ,  $\Omega_O$  and  $\Omega_{H1} \cup \Omega_{H2}$  domains, the three-basin EDF shown in Figure 6 arises. In it, the EDF probabilities are grouped according to the number of electrons in  $\Omega_{H1} \cup \Omega_{H2}$  ( $n_{HH}$ ), giving rise to “sub-EDFs” within the general EDF. Each of them defines a distribution of  $16 - n_{HH}$  electrons between two domains:  $\Omega_C$  and  $\Omega_O$ . The five sub-EDF’s plotted in Figure 6, which associate from 12 to 16 electrons to the carbonyl group ( $n_{CO} = 16 - n_{HH}$ ), account for more than 99% of the distribution in both  $S_0$  and  $S_1$  states. The sub-EDF with a neutral carbonyl moiety is the most important in both states (37.38 and 36.38 %, respectively) and its maximum is also the absolute maximum of the whole three-basin EDF, corresponding to the ionic  $(\text{H}_2)^0\text{C}^+\text{O}^-$  RSRS in both states.

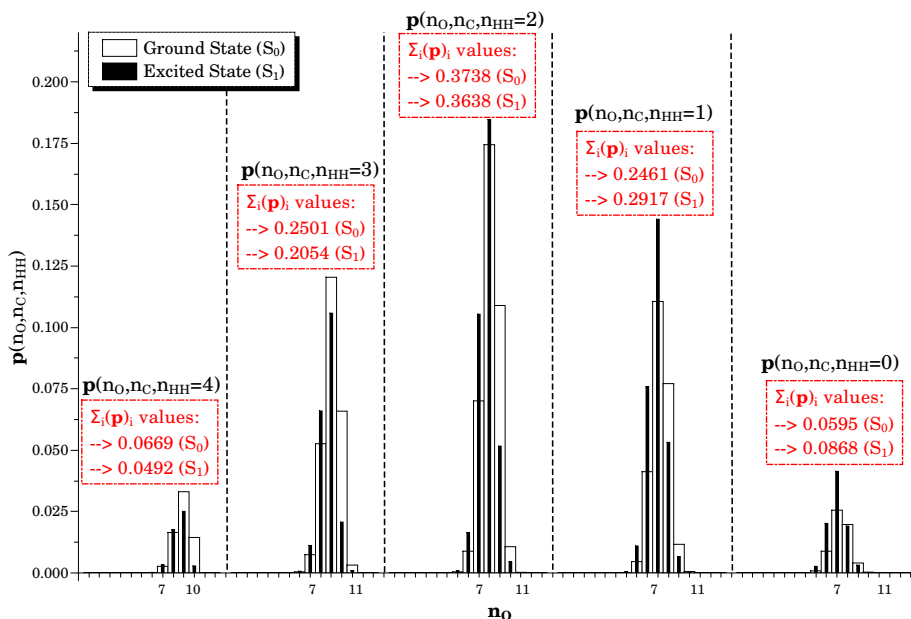


Figure 6: Most significant components of the three-basin EDF for formaldehyde at the SA-CASSCF(AS-IV) level of calculation, grouped according to the number of electrons associated to the  $\Omega_{H1} \cup \Omega_{H2}$  domain ( $n_{HH}$ ). Notice that the electrons within  $\Omega_C \cup \Omega_O$  ( $n_{CO}$ ) for each group is given by  $n_{CO} = 16 - n_{HH}$ . Values inside dash-dot squares,  $\sum_i(\mathbf{p})_i$ , correspond to  $\sum_{i=0}^{16-n_{HH}} \mathbf{p}(i, 16 - n_{HH} - i, n_{HH})$ .

The contribution of each subEDF generates the distribution of electrons between HH and CO domains (values within dash-dot squares in Figure 6). This two-basin EDF is almost symmetric with respect to the  $(H_2)^0(CO)^0$  neutral structure for the ground state. Upon electronic excitation, this pseudo-symmetry is broken and the probability for RSRS's with negatively-charged carbonyl group increases, basically at the expense of the positively-charged ones. As a consequence, the net charge of the CO moiety is almost neutral (slightly positive) in the ground state (+0.0297 au), whereas it turns clearly negative in the excited state (-0.1520 au). Furthermore, the decrease of the sub-EDF skewnesses (Figure 6) confirms the enhancement of the C electronegativity in the  $S_1$  state.

The re-normalization of the sub-EDF's allows the calculation of the average number of electrons in  $\Omega_O$  (Figure 7a) as well as of the delocalization index between  $\Omega_C$  and  $\Omega_O$  (Figure 7b) for a given number of electrons within the CO fragment. In such wise, the behavior of the CO unit as electrons are pumped (one by one) from the hydrogens to it can be analyzed (Figure 7c):  $(H_2)^{-a}(CO)^{+a} \rightarrow (H_2)^{-a+1}(CO)^{+a-1} \rightarrow \dots \rightarrow (H_2)^{+2}(CO)^{-2}$ , with  $a$  being the initial positive (integer) charge associated to the carbonyl group at the beginning of such a process. Our starting RSRS is  $(H_2)^{-7}(CO)^{+7}$  and five of the seven electrons associated to the carbonyl group are situated in the oxygen basin (Figure

7a). This clearly exemplifies the strong appetite of oxygen for electrons. Moreover, each of the first four electrons introduced in the pumping-process ends up belonging basically to the oxygen basin (in order: 92, 88, 85, and 78 %). Once these four electrons are pumped from hydrogens, oxygen presents an averaged electron population of 8.3787 electrons, whereas the C atom only owns 2.6213 electrons. At this point, we observe that oxygen is close to its electron-saturation limit: its electron population slightly increases when more electrons are introduced into the CO fragment. In other words, its electron-appetite decreases and, consequently, the ability of C to attract electron density enhances. Specifically, the next electron is almost equally distributed between O and C and the subsequent ones are basically introduced inside the C basin. The variation of the delocalization index with the number of electrons also presents a change at a carbonyl electron population of eleven. Its increase is more pronounced at the beginning, indicating that the role of the first electrons is basically centered in the formation of the bond.

Upon electronic excitation, the atomic abilities to attract electron density are similar in the first steps of the process, but the electron saturation limit decreases for oxygen (increases for carbon), which indicates again that the relative electronegativity ( $\chi_r = \chi_O - \chi_C$ ) between O and C is smaller in  $S_1$ . The behavior of the delocalization index (Figure 7b) indicates that the electronic excitation only modifies significantly the bonding structure for the  $(H_2)^{-2}(CO)^{+2}$  to  $(H_2)^+(CO)^-$  RSRS's.

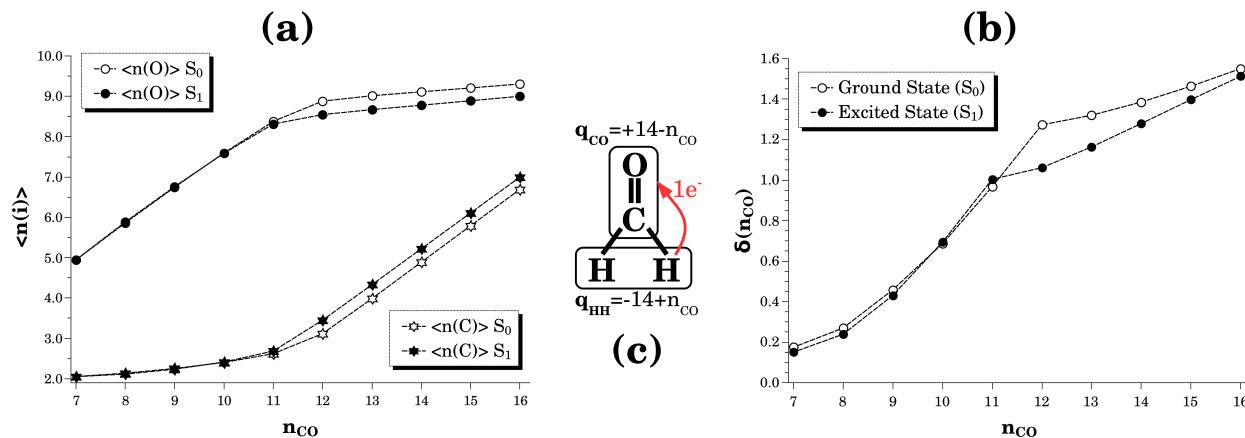


Figure 7: Averaged value of O and C electron population (a) and delocalization index (b) associated to diverse  $p(n_O, n_C, n_{HH})$  distributions, generated after grouping according to constant values of  $n_{HH}$  (see Figure 6). The abscissa is labeled with the value of  $n_{CO}$ , which is related to  $n_{HH}$  through:  $n_{CO} + n_{HH} = 16$ . Data correspond to the SA-CASSCF(AS-IV) wave function.

We remark how the huge amount of chemical information stored in EDFs may be extracted with clever procedures. Through the curious theoretical process just described, we have got information about the ability of the atoms to attract the electron density toward themselves as well as about their

electron saturation limit and how it changes upon electronic excitation.

## 5 Conclusions

Application of the topological approach to electronically excited states allows extracting information to improve chemical knowledge. Undoubtedly, all this wisdom can be crucial to design synthetic routes involving steps in these excited states. This is a long-term project, so analyses of prototypical systems, such as the test results here reported, are still in need before getting to such far-reaching goals.

In this work, we have analyzed the EDF of formadehyde in terms of (2c,2e) links, relating them to orbital entities. Among the results, we highlight that:

- We find that the  $\sigma$  link contributes less to the total delocalization index of the CO double bond than the  $\pi$  link. This behavior can be related to the fact that the  $\sigma$  electron density is more sensitive to electronegativity effects, as it is more confined among the nuclei than the  $\pi$  density.
- There is an important misconception regarding antibonding orbitals. Their population does not imply, necessarily, a decrease in the delocalization index of the corresponding bond. As an example, we have considered a model picture for the electronic  $S_0 \rightarrow S_1$  transition. In this orbital-frozen image, the consideration of electron distribution functions to describe the electron jump from an oxygen lone pair to a  $\pi_{CO}^*$  orbital ends up increasing the CO delocalization index. Indeed, a SA-CASSCF(2,2) calculation, which is close to this idyllic picture, confirms this prediction. The decrease in the delocalization index arises from other terms in the wave function, where the population of  $\pi_{CO}^*$  is made at the expenses of the  $\pi_{CO}$  orbital.
- The electronic  $S_0 \rightarrow S_1$  transition is understood, in terms of orbitals, as an electron jump from the oxygen lone pair to the  $\pi_{CO}^*$  orbital. The DAFH analysis provides us with an alternative conception: the transition can be considered as a rotation of one averaged electron in the oxygen lone pair. As a consequence of this transition, an overlap is generated between the new distribution of the electron and the  $\pi$  density of the CO bond. The huge repulsion moves part of this  $\pi$  electron density towards C, giving rise to a lone pair-like distribution of one averaged electron situated in C.
- The consideration of the electronegativity index  $g_{\Omega\Omega'}$  allows us to state that the relative effective electronegativity of C increases upon excitation to  $S_1$ .

From the three-basin EDF, we also observe that:

- The neutral character of the CO group in  $S_0$  is not only a consequence of the significance of the neutral  $(\text{H}_2)^0(\text{CO})^0$  RSRS, but also of the equiprobability of the  $(\text{H}_2)^-(\text{CO})^+$  and  $(\text{H}_2)^+(\text{CO})^-$  structures. Upon excitation, the weight of the neutral form remains almost invariant, but that of the  $(\text{H}_2)^+(\text{CO})^-$  increases at the expenses of the cationic one.
- A curious process of electron pumping from hydrogens to the CO moiety has been analyzed through the three-basin EDF. In it, we can quantitatively observe the saturation limit of the oxygen atom, which decreases upon excitation, as well as the important role of the  $(\text{H}_2)^{-2}(\text{CO})^{+2}$  to  $(\text{H}_2)^+(\text{CO})^-$  RSRS's in the bonding structure of the excited  $S_1$  state.

## 6 Acknowledgments

D. F-C. and R. A. M. thank Spanish Ministry of Economy for project CTQ2010-21500. D. F-C. also thanks Spanish Ministry of Education for an FPU fellowship and M. Castiñeira for her continued support. EF and AMP also thank the Spanish MINECO, grant CTQ2012-31174, for financial support.

## References

- [1] P. L. Ayers, R. J. Boyd, P. Bultinck, M. Caffarel, R. Carbó-Dorca, M. Causá, J. Cioslowski, J. Contreras-Garcia, D. L. Cooper, P. Coppens, C. Gatti, S. Grabowsky, P. Lazzeretti, P. Macchi, Á. M. Pendás, P. L. A. Popelier, K. Ruedenberg, H. Rzepa, A. Savin, A. Sax, W. H. E. Schwarz, S. Shahbazian, B. Silvi, M. Solà and V. Tsirelson, *Comput. Theor. Chem.*, 2015, **1053**, 2 – 16.
- [2] P. L. A. Popelier, *Struct. Bond.*, 2005, **115**, 1–56.
- [3] R. F. W. Bader, *Atoms in Molecules: A Quantum Theory*, Clarendon Press, Oxford, 1995.
- [4] R. F. W. Bader, *Chem. Rev.*, 1991, **91**, 893–928.
- [5] A. D. Becke and K. E. Edgecombe, *J. Chem. Phys.*, 1990, **92**, 5397 – 5403.
- [6] B. Silvi and A. Savin, *Nature*, 1994, **371**, 683 – 686.
- [7] E. Chamorro, P. Fuentealba and A. Savin, *J. Comput. Chem.*, 2003, **24**, 496 – 504.
- [8] E. Cancès, R. Keriven, F. Lodier and A. Savin, *Theor. Chem. Acc.*, 2004, **111**, 373 – 380.
- [9] E. Francisco, A. Martín Pendás and M. A. Blanco, *J. Chem. Phys.*, 2007, **126**, 094102.

- [10] A. Martín Pendás, E. Francisco and M. A. Blanco, *J. Chem. Phys.*, 2007, **127**, 144103.
- [11] E. Francisco and A. Martín Pendás, *Comput. Phys. Commun.*, 2014, **185**, 2663 – 2682.
- [12] R. Ponec, *J. Math. Chem.*, 1997, **21**, 323–333.
- [13] R. Ponec, *J. Math. Chem.*, 1998, **23**, 85–103.
- [14] E. Francisco, A. Martín Pendás and M. A. Blanco, *J. Chem. Phys.*, 2009, **131**, 124125.
- [15] E. Francisco, A. Martín Pendás and A. Costales, *Phys. Chem. Chem. Phys.*, 2014, **16**, 4586–4597.
- [16] P. Cassam-Chenaï and D. Jayatilaka, *Theor. Chem. Acc.*, 2001, **105**, 213–218.
- [17] D. Ferro-Costas, A. Martín Pendás, L. González and R. A. Mosquera, *Phys. Chem. Chem. Phys.*, 2014, **16**, 9249–9258.
- [18] A. Martín Pendás, E. Francisco and M. A. Blanco, *Phys. Chem. Chem. Phys.*, 2007, **9**, 1087–1092.
- [19] R. McWeeny, *Methods of Molecular Quantum Mechanics*, Academic Press, London, 1992.
- [20] J. Cioslowski, *Int. J. Quantum Chem.*, 1990, **S24**, 15 – 28.
- [21] B. O. Roos, P. R. Taylor and P. E. M. Siegbahn, *Chem. Phys.*, 1980, **48**, 157–173.
- [22] M. A. Blanco, A. M. Pendás and E. Francisco, *J. Chem. Theory Comput.*, 2005, **1**, 1096–1109.
- [23] M. J. Frisch, G. W. Trucks, H. B. Schlegel, G. E. Scuseria, M. A. Robb, J. R. Cheeseman, G. Scalmani, V. Barone, B. Mennucci, G. A. Petersson, H. Nakatsuji, M. Caricato, X. Li, H. P. Hratchian, A. F. Izmaylov, J. Bloino, G. Zheng, J. L. Sonnenberg, M. Hada, M. Ehara, K. Toyota, R. Fukuda, J. Hasegawa, M. Ishida, T. Nakajima, Y. Honda, O. Kitao, H. Nakai, T. Vreven, J. A. Montgomery, Jr., J. E. Peralta, F. Ogliaro, M. Bearpark, J. J. Heyd, E. Brothers, K. N. Kudin, V. N. Staroverov, R. Kobayashi, J. Normand, K. Raghavachari, A. Rendell, J. C. Burant, S. S. Iyengar, J. Tomasi, M. Cossi, N. Rega, J. M. Millam, M. Klene, J. E. Knox, J. B. Cross, V. Bakken, C. Adamo, J. Jaramillo, R. Gomperts, R. E. Stratmann, O. Yazyev, A. J. Austin, R. Cammi, C. Pomelli, J. W. Ochterski, R. L. Martin, K. Morokuma, V. G. Zakrzewski, G. A. Voth, P. Salvador, J. J. Dannenberg, S. Dapprich, A. D. Daniels, Ö. Farkas, J. B. Foresman, J. V. Ortiz, J. Cioslowski and D. J. Fox, *Gaussian 09 Revision A.02*, Gaussian Inc. Wallingford CT 2009.

- [24] T. H. Dunning, *J. Chem. Phys.*, 1989, **90**, 1007–1023.
- [25] D. Ferro-Costas and R. A. Mosquera, *Phys. Chem. Chem. Phys.*, 2015, **17**, 7424–7434.
- [26] D. Ferro-Costas, I. Pérez-Juste and R. A. Mosquera, *J. Comput. Chem.*, 2014, **35**, 978–985.
- [27] D. Ferro-Costas, N. Ramos-Berdullas and R. A. Mosquera, *Comput. Theor. Chem.*, 2015, **1053**, 85–89.